BOREAL ENVIRONMENT RESEARCH 20: 526–541
ISSN 1239-6095 (print) ISSN 1797-2469 (online)

Helsinki 28 August 2015

Long-term variability of aerosol optical properties in northern Finland

Heikki Lihavainen, Antti Hyvärinen, Eija Asmi, Juha Hatakka and Yrjö Viisanen

Finnish Meteorological Institute, P.O. Box 503, FI-00101 Helsinki, Finland

Received 6 Aug. 2014, final version received 13 Mar. 2015, accepted 16 Mar. 2015

Lihavainen H., Hyvärinen A., Asmi E., Hatakka J. & Viisanen Y. 2015: Long-term variability of aerosol optical properties in northern Finland. *Boreal Env. Res.* 20: 526–541.

We studied the optical properties in continental and marine air masses, including seasonal cycles and long-term trends using 10-year data on aerosol scattering properties and 5-year data on absorption and combined aerosol optical properties. The average (median) scattering coefficient, backscattering fraction, absorption coefficient and single scattering albedo at the wavelength of 550 nm were 7.9 (4.4) Mm^{-1}, 0.13 (0.12), 0.74 (0.35) Mm^{-1} and 0.92 (0.93), respectively. We observed clear seasonal cycles in these variables, the scattering coefficient having high values during summer and low in autumn, and absorption coefficient having high values during winter and low in autumn. We found that the high values of the absorption coefficient and low values of the single scattering albedo were related to continental air masses from lower latitudes. These aerosols can induce an additional effect on the surface albedo and melting of snow. We observed the signal of the Arctic haze in marine (northern) air masses during March and April. The haze increased the value of the absorption coefficient by almost 80% and that of the scattering coefficient by about 50% compared with the annual-average values. We did not observe any long-term trend in the scattering coefficient, while our analysis showed a clear decreasing trend in the backscattering fraction and scattering Ångström exponent during winter. A possible reason for this feature is the gradual change in the relative contributions of different emission sources. However, this remains to be confirmed by future studies.

Introduction

Aerosols are well recognized for their important effects on air quality and climate (e.g. Charlson *et al*. 1992). Despite considerable progress in atmospheric models, and observational systems and networks, large uncertainties in the direct radiative forcing caused by anthropogenic aerosols still exist (e.g., Bellouin *et al*. 2008, Quaas *et al*. 2008 Zhout *et al*. 2012). The uncertainties in various climate effects of aerosols continue to be the largest uncertainty in the total, global radiative forcing estimate (IPCC 2013).

Aerosol optical properties, along with some non-aerosol properties like the surface albedo and solar declination angle, are key factors when investigating the direct radiative effects of atmospheric aerosols. Because of their various sources and short life-times, the properties of atmospheric aerosols may vary significantly in both time and space. In addition to the changes occurring on short time-scales, the aerosol opti-

Editor in charge of this article: Veli-Matti Kerminen

cal properties also vary on decadal scales, especially at lower latitudes (Collaud Coen *et al*. 2013).

Continuous long-term measurements of aerosol optical properties, such as the scattering and absorption coefficients, have not been extensively reported. The published studies include measurements made at coastal sites (e.g. Sheridan and Ogren 1999, Delene and Ogren 2002, Vaishya *et al*. 2012), in the free troposphere (e.g. Sheridan and Ogren 1999), in a primary forest in Amazonia (Rizzo *et al*. 2013), in a boreal forest (Virkkula *et al*. 2013), in Arctic regions (e.g. Delene and Ogren 2002, Treffeisen *et al*. 2004, Aaltonen *et al*. 2006) and in areas with a high sulfate burden (e.g. Delene and Ogren, 2002). High Arctic aerosol loadings, i.e. Arctic haze, have also been investigated (e.g. Beine *et al*. 1996, Heintzenberg *et al*. 2003, Treffeisen *et al*. 2004). Collaud Coen *et al*. (2013) studied long-term aerosol trends at a few Arctic and Antarctic locations, from which more than 10 years of aerosol optical data were available. They did not find any significant trends in the scattering coefficient, whereas a negative trend in the absorption coefficient was found for the Arctic stations.

Arctic areas are estimated to warm twice as fast than the rest of the globe, and it was recently estimated that aerosols may have contributed to more than half of the observed Arctic warming since 1890, most of this occurring during the last three decades (Shindell and Faluvegi 2009). There are still large uncertainties associated with emissions of aerosols to the atmosphere, their aging during atmospheric transportation, and their removal by precipitation and other deposition mechanisms. Although optical properties of aerosols have been studied in several regions, there is still a need for long-term measurements, especially in remote or moderately-polluted environments. In this study, we present results from simultaneous aerosol scattering and absorption measurements made at the Pallas Global Atmospheric Watch station. Aaltonen *et al*. (2006) analyzed the first three years of the measurements of the scattering coefficient and presented how this scattering coefficient is related to the measured particle number size distribution. Hyvärinen *et al*. (2011) analyzed black carbon concentrations measured at Pallas and four other sites in Finland. They used the same instrument as we used in this work, though we report the results in more climate-relevant units, such as an absorption coefficient. In this paper, analyses of ten years of scattering coefficient (2001–2010), and five years of absorption coefficient (2006–2010) and combination of scattering and absorption coefficient data, along with their relationship, are presented. We investigated how marine and continental air masses affect the aerosol optical properties and analyze long-term trends of different aerosol properties derived from the measured scattering coefficients. We hypothesized that the decreased anthropogenic emissions of e.g. soot, NO_x and SO_2 during the last 10 years have led to substantial changes in aerosol optical properties at Pallas. We further hypothesized that the emission sources were different in different seasons, influencing thereby climate through different pathways in different times of the year. Finally, we investigated whether the effect of Arctic haze could be observed at our measurement site.

Methods

Site description

A detailed site description can be found in Hatakka *et al*. (2003), so only a short overview is given here. The analyzed data were gathered at the Pallas Global Atmosphere Watch station, the Sammaltunturi measurement site located in northern Finland (67°58´N, 24°07´E; Fig. 1), in a subarctic region. The station is hosted by the Finnish Meteorological Institute. The Sammaltunturi station lies on a top of a fjeld, a round-topped treeless hill, in a 50-km-long north–south chain of fjelds at an elevation of 565 m a.s.l.. The vegetation on the fjeld top is sparse, consisting mainly of low vascular plants, moss and lichen. The Sammaltunturi station is about 300 m above the surrounding area and the tree line lies about 100 m below the station. The surrounding forest consists of pine, spruce and birch. The tops of the highest fjelds in the chain reach 600–800 m a.s.l. Otherwise, the region is hilly (250–400 m a.s.l.), forested and partly swampy with some rather large lakes at about 250 m a.s.l. The

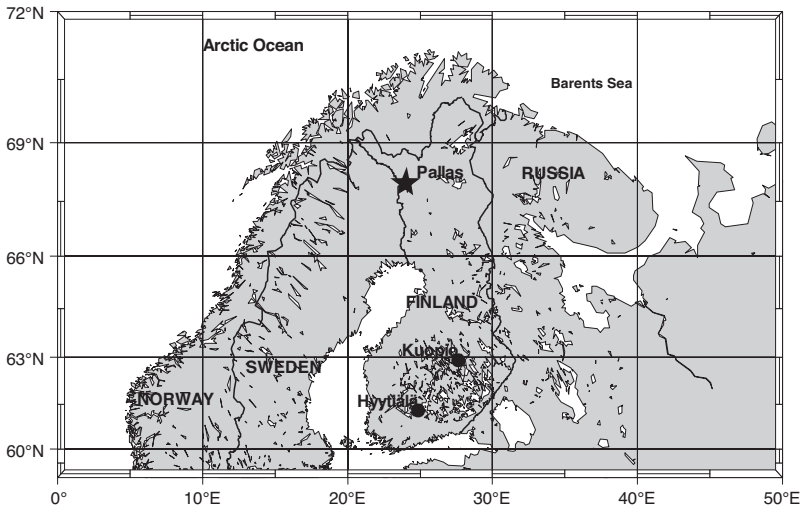

Fig. 1. Location of the Pallas GAW station. Also marked two other continuous aerosol scattering and absorption measurement sites, Kuopio and Hyytiälä.

station is located inside the Pallas–Yllästunturi National Park (total area 1020 km^2).

Measurements

The scattering and backscattering coefficients were measured with an integrating nephelometer (model 3563, TSI, Inc., St. Paul, Minnesota). This instrument measures scattering by aerosols at three wavelengths: 450, 550 and 700 nm. The inlet of the main sampling line is about 3 m above the roof of the station building and about 7 m above the ground. The calculated (Baron and Willeke 2001) cut-off diameter of the inlet nozzle and sample transport lines was about 5 μm. A detailed description of the inlet and the measurement system can be found in Komppula *et al*. (2005) and Aaltonen *et al*. (2006). The inlet system was modified in August 2005 when the sampling line was changed and $PM_{2.5}$ (particles < 2.5 μm in diameter) nozzle was applied. The inlet nozzle was later replaced with a PM_{10} (particles < 10 μm in diameter) in January 2008 when the sample line was additionally equipped with a nafion dryer (manufacturer Dekati, model DD-600). We may assume that these changes have had only minor effects on the scattering coefficient, because the number concentration of coarse particles is very low at Pallas. Non-idealities due to non-lambertian and truncation errors in the nephelometer were corrected using the method described by Anderson and Ogren (1998). The nephelometer was calibrated with CO_2 and zero air approximately every other month and the light source was changed every half a year. The zero air calibration is automatically done every hour. The measurements were made according to the guidelines of the GAW recommendation. We excluded the scattering data when the relative humidity inside the nephelometer was higher than 50%.

The absorption coefficient was measured with Aethalometer (Magee Scientific, model AE31). It measures absorption at seven wavelengths: 370, 470, 520, 590, 660, 880, and 950 nm. The Aethalometer absorption measurement is known to suffer from a filter-loading artifact. This artifact can be corrected using different methods. Here, the approach presented by Weingartner *et al*. (2003) was chosen. In the original method, the correction factor, C, is equal to 2.14. At Sammaltunturi there is also a MAAP (Multi Angle Absorption Photometer, Thermo Anderssen). It was installed in August 2007. Here, we used the Aethalometer data because of its longer data set, and because of the possibility to study the absorption wavelength dependency. The MAAP was considered more reliable than Aethalometer in absorption measurements, so we used it to calculate a new correction factor, C_{ref}. The black carbon concentration obtained from the MAAP was converted into absorption at 637 nm using the method presented by Müller *et al*. (2011).

Two years of absorption data gathered by these two devices at 637 nm were then compared, and by fitting a LST curve between the MAAP and Aethalometer measurements resulted in

$$\sigma_{MAAP} = (0.562 \pm 0.001)\sigma_{AE} - (0.040 \pm 0.002). \quad (1)$$

The regression coefficient of the fitting was 0.99. The new correction factor was defined by using the slope of the fitted curve as $C_{ref} = C/0.56 = 2.14/0.56 = 3.8$.

Weather variables were measured with an automatic weather station. The measured variables were air temperature, pressure, relative humidity, wind speed and wind direction. At the Sammaltunturi station, there were also sensors for visibility and total global radiation. The cloud fraction and the height of cloud layers were measured using a ceilometer (Vaisala, model CT25K). This instrument was at a nearby measurement site, Kenttärova, at an elevation lower by about 200 m and 7 km east of the Sammaltunturi station.

Data processing

Scattering measurements at Sammaltunturi were started in April 2000 and absorption measurements at seven wavelengths with the Aethalometer were started in August 2005. The data were first quality-checked against peculiar events, such as extreme high or low concentrations, which might have been caused, for example, by an instrument malfunction. The station logbook was used to remove obvious local man-made emissions during the station visits. The time resolution of the measurements was five minutes. Hourly averages were calculated if more than 50% of the data existed inside the hour in question. The Sammaltunturi station is occasionally inside a cloud. We filtered out all the data that had an hourly average visibility lower than 5000 m. During the measurement period, the visibility was below 5000 m for about 20% of the time. Cases when the visibility sensor was not functioning properly were also removed, which disqualified 13% of the data. Most of these cases were caused by the snow and ice covering the sensor. Additional 10% of the data were lost because of instrumental or infrastructure-caused malfunctions. The final data coverage after this pre-selection and quality assurance was about 50%. The data are reported in STP conditions.

Valid data were not equally distributed between the seasons. The harsh weather conditions during late autumn and winter resulted in more data being missing from those periods, putting thus higher emphasis on spring and summer data in annual-average values. We compensated this bias by first calculating the monthly averages for those months with higher than 30% data coverage. Long-term monthly averages were calculated using these values and the overall-average scattering variables were further derived from these monthly averages.

The five-minute detection limits for the total scattering coefficients were 0.44, 0.17, and 0.26 Mm^{-1} at the wavelengths of 450, 550, and 700 nm, respectively (Anderson *et al*. 1996), and for backscattering the corresponding detection limits were 0.29, 0.11, and 0.21 Mm^{-1}. These limits were disregarded in calculation of averages, since otherwise it would again cause a bias towards higher values. Negative values were, however, removed because they are not applicable in the correction method (Anderson and Ogren 1998). The effect of this procedure to the final results was only minor (< 3%).

The aethalometer and nephelometer measure the aerosol optical properties at slightly different wavelengths. For further analysis, the absorption coefficients were calculated at same wavelengths as the nephelometer is measuring (450, 550 and 750 nm) by fitting a curve to the equation,

$$\sigma_{abs} = K\lambda^{\mathring{a}_{abs}}, \quad (2)$$

where λ is the wavelength, and K and $\mathring{a}_{abs}$ are constants. The quantity $\mathring{a}_{abs}$ is also called the absorption Ångström coefficient, and it is sometimes used in analysing the sources of absorbing aerosols.

The backscattering fraction, b, was calculated from

$$b(\lambda) = \frac{\sigma_{bsc}(\lambda)}{\sigma_{sca}(\lambda)}, \quad (3)$$

where σ_{sca} and σ_{bsc} are the scattering and backscattering coefficients, respectively. The greater

the value of b is, the larger fraction of incoming solar light is scattered back to space.

The Ångström exponent for absorption, $\mathring{a}_{abs}$, was calculated using Eq. 1, and the Ångström exponent for scattering, $\mathring{a}_{sca}$, was calculated as

$$\mathring{a}_{sca} = -\frac{\log\sigma_{sca}(700\text{ nm}) - \log\sigma_{sca}(450\text{ nm})}{\log 700 - \log 450}. \quad (4)$$

A large value of $\mathring{a}_{sca}$ corresponds to a particle size distribution with scattering dominated by submicron particles, whereas a size distribution dominated by coarse particles has typically a small value of $\mathring{a}_{sca}$.

Air mass analysis

The data were divided according to their air mass history into two categories: marine and continental. We used air mass back trajectories calculated with the FLEXTRA trajectory model (e.g. Stohl and Seibert 1998) and data from the European Center for Medium-Range Weather Forecasts (ECMWF). A trajectory was calculated for every 3 h and it extended 120 h backward in time. Combining trajectories with the hourly-average scattering data led to 43 906 data pairs, and combining trajectories with the absorption data led to 16 530 data pairs (Table 1). For the absorption coefficient, 28 370 pairs were obtained. The trajectory was defined as marine if it had spent more than 70% of its time over marine areas and continental if it had spent less than 50% of its time in the marine sector (Tables 2 and 3). The limit of only 50% was selected because most of these air masses had spent their last 60 hours over continental areas prior to arriving at the station, which was considered sufficient to detect the continental features.

Determination of trends

We selected the following four periods for the trend analysis: winter, Arctic haze (spring) period, summer and autumn. Winter was defined as the two coldest and darkest months of the year (January and February). The Arctic-haze period covers the late winter and early spring (March and April). The same period was also used by Quinn *et al*. (2007) in their analysis, though they analyzed these two months separately. Summer was defined as the two warmest months having also plenty of daylight (July and August). For technical reasons autumn was defined as September and October. Most of the data gaps due to

Table 1. Numbers of hourly-average data points used in the calculations (n), means, standard deviations (SD) and median values of the analyzed variables, as well as means ($Mean_{mo}$) and standard deviations (SD_{mo}) calculated from the monthly-average values of the same variables. The scattering (σ_{sca}) and absorption coefficients (σ_{abs}) are given in Mm^{-1} and converted to the conditions 1013 mbar and 273.15 K. The values of σ_{sca}, backscatter fraction (b) and Ångström exponent of scattering ($\mathring{a}_{sca}$) were calculated from the data covering the years 2001–2010, and the values of σ_{abs}, Ångström exponent of absorption ($\mathring{a}_{abs}$) and single-scattering albedo (SSA) were calculate from the data covering the years 2005–2010. The numbers in the parenthesis refer to the wavelength.

	n	Mean	SD	Median	$Mean_{mo}$	SD_{mo}
σ_{sca} (450 nm)	43906	11.2	14.0	6.0	9.7	4.2
σ_{sca} (550 nm)	43906	7.8	9.6	4.4	6.9	2.6
σ_{sca} (700 nm)	43906	4.9	5.7	3.0	4.4	1.4
b (450 nm)	43906	0.12	0.05	0.11	0.10	0.01
b (550 nm)	43906	0.13	0.03	0.12	0.12	< 0.01
b (700 nm)	43906	0.17	0.06	0.17	0.16	< 0.01
σ_{abs} (450 nm)	28370	0.93	1.37	0.44	0.90	0.60
σ_{abs} (550 nm)	28370	0.74	1.10	0.35	0.72	0.48
σ_{abs} (700 nm)	28370	0.57	0.84	0.27	0.55	0.37
SSA (450 nm)	16530	0.92	0.05	0.93	0.92	0.04
SSA (550 nm)	16530	0.92	0.05	0.93	0.91	0.04
SSA (700 nm)	16530	0.90	0.06	0.91	0.90	0.04
$\mathring{a}_{sca}$	43906	1.7	0.7	1.8	1.6	0.3
$\mathring{a}_{abs}$	28370	1.1	0.6	1.1	1.1	0.1

low clouds and low visibility were encountered in late autumn and early winter, therefore leaving only these two months with sufficient amount of data for our analysis.

Yearly averages were calculated for each period for the whole data set and for marine and continental air masses. A non-parametric Mann-Kendall test with Sen's method of slope evaluation (Gilbert 1987) was applied to each case for σ_{sca} at 550 nm, $\mathring{a}_{sca}$ (between 700 and 450 nm) and b at 550 nm.

Results and discussion

Weather

Most meteorological variables had a clear seasonal cycle during the 10-year measurement period (Fig. 2). The lowest monthly-average temperatures of about –10 °C were observed in January–February, and during the coldest days the daily-average temperatures were around –26 °C. The mean temperature of the warmest months (July–August) was about 12 °C, with daily means reaching 23 °C. The monthly-mean relative humidity (RH) was higher than 90% between October and February, and had a minimum of around 70% in June. The wind speed and direction had a weak seasonal cycle. The monthly-mean local wind speed (WS) varied between about 5 and 7 m s^{-1}, while the maximum one-hour-average wind speed was 26 m s^{-1}. The highest wind speeds were typically related to the sectors 60°–80° and 270°–300°, and the monthly-mean wind direction varied in the range 160°–200°. Visibility, which was also used to filter out cases when the station was inside a cloud, had highest values during summer and lowest during autumn and winter. The visibility varied between few tens of meters and 50 km which is the upper limit of the instrument.

Common features of aerosol optical properties

A clear seasonal cycle was found in both the scattering coefficient, σ_{sca}, and the absorption coefficient, σ_{abs}, at 550 nm (Fig. 3). There were a few long gaps in the data due to malfunction of the instrument, and the larger amount of missing data from the winter season compared with the summer and spring seasons clearly affected

Table 2. The same as in Table 1, except for marine air masses and wavelength of 550 nm only.

Marine	*n*	Mean	SD	Median	Mean (monthly)	SD (monthly)
σ_{sca} (550 nm)	6654	4.1	5.7	2.7	3.9	1.1
b (550 nm)	6654	0.13	0.04	0.12	0.12	< 0.01
σ_{abs} (550 nm)	4111	0.28	0.32	0.19	0.28	0.13
SSA (550 nm)	2955	0.92	0.05	0.93	0.93	0.02
$\mathring{a}_{sca}$	665	1.4	0.7	1.4	1.3	0.3
$\mathring{a}_{abs}$	4111	1.1	0.7	1.0	1.1	0.2

Table 3. The same as in Table 1, except for continental air masses and wavelength of 550 nm only.

Continental	*n*	Mean	SD	Median	Mean (monthly)	SD (monthly)
σ_{sca} (550 nm)	4876	13.6	12.05	10.4	11.4	4.1
b (550 nm)	4876	0.13	0.03	0.13	0.12	0.01
σ_{abs} (550 nm)	4072	1.29	1.44	0.76	1.26	0.78
SSA (550 nm)	1809	0.91	0.05	0.92	0.89	0.04
$\mathring{a}_{sca}$	4876	2.0	0.4	2.1	1.9	0.2
$\mathring{a}_{abs}$	4072	1.1	0.4	1.1	1.1	0.1

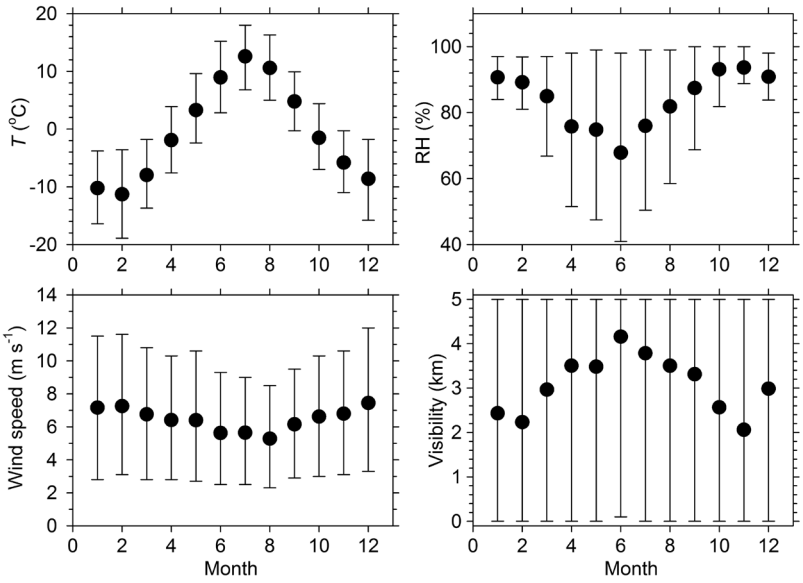

Fig. 2. Seasonal cycle of temperature (*T*), relative humidity (RH), wind speed and visibility. The dots represent monthly-average values for the 10-year period, 2001–2010, and the bars represent the 10–90 percentile range.

the mean values (*see* Table 1). When using the hourly-average data directly, the mean value of σ_{sca} at 550 nm was 7.8 Mm^{-1}, which is about 15% higher than the value of 6.9 Mm^{-1} obtained using monthly-average data in order to compensate for the poor data coverage during autumn and winter. The method of averaging affected the results about equally at all the scattering wavelengths. In case of absorption, the mean value of σ_{abs} at 550 nm calculated from the hourly-average data was 0.74 Mm^{-1}, while when compensating for poor autumn and winter data coverage, this value decreased by 3% to 0.72 Mm^{-1}. Again, a similar difference was found for all the three wavelengths as a result of the low absorption values during autumn and early winter.

The highest one-hour average value of σ_{sca} at 550 nm was 176 Mm^{-1} on 30 July 2010, and the corresponding value of σ_{abs} was also quite high, about 5 Mm^{-1}. Back-trajectories suggest that these high values were related to extensive forest fires in Russia. This particular case was analyzed in more detailed by Mielonen *et al*. (2013). The maximum value of σ_{abs} at 550 nm was 13 Mm^{-1}, observed on 25 August 2005, coinciding with a high σ_{sca} of about 87 Mm^{-1}. On the same day in visibility decreased to about 10 km. Wildfire maps and back-trajectories suggest that the origin was again wildfires in Russia and eastern Europe.

Compared with an earlier study by Aaltonen *et al*. (2006) which was based on three years of measurement at Pallas, the mean value of σ_{sca} in this study differs by less than 10%. Aaltonen *et al*. (2006), however, reported these values under ambient conditions. When the scattering coefficients reported by Aaltonen *et al*. (2006) are transformed to the STP conditions by using average temperatures and pressures, the difference in the mean values of σ_{sca} decreases to around 5%.

At the Hyytiälä forestry field station in southern Finland, located 680 km south of Pallas, the average reported scattering coefficients were more than two times those at Pallas and the absorption coefficients were about three times those at Pallas, depending on wavelength (Virkkula *et al*. 2011). It should, however, be noted that Virkkula *et al*. (2011) calculated the absorption coefficients slightly differently than here. At a semi-urban station at the Puijo tower in Kuopio, located 590 km south of Pallas and 210 km northeast from Hyytiälä (Fig. 1), the scattering coefficients were about 1.4 times those at Pallas (Leskinen *et al*. 2012). In summary, these results from different locations in Finland indicate that both σ_{sca} and σ_{abs} are higher at lower latitudes where anthropogenic emissions and impact of long-way transported pollution from Europe is higher. Also the natural aerosol load is likely to increase towards the south due to higher temperatures and

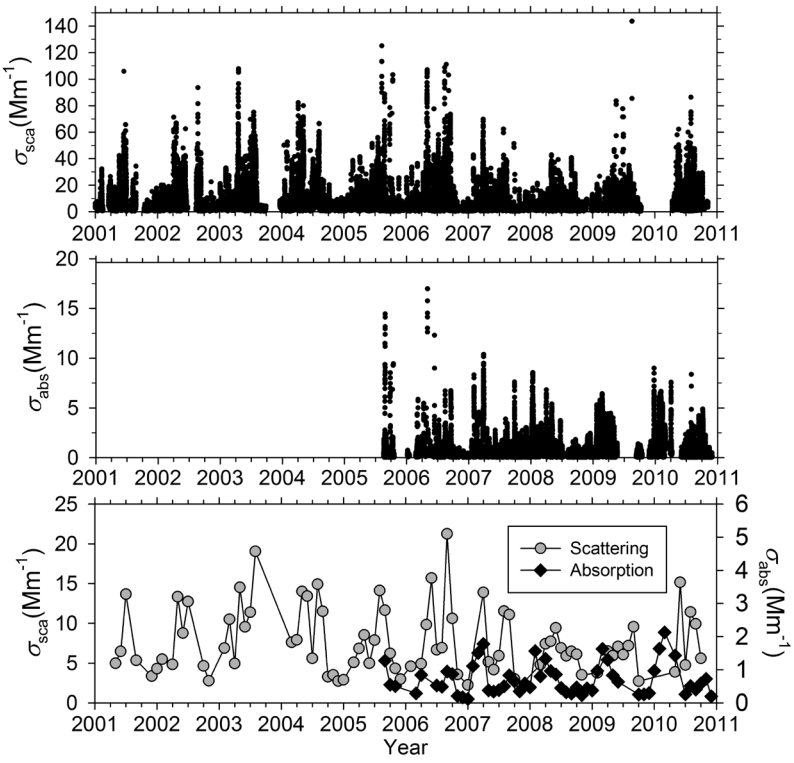

Fig. 3. Hourly averages of the scattering coefficient, σ_{sca} (top), hourly averages of the absorption coefficient, σ_{abs} (middle) and monthly averages of σ_{sca} and σ_{abs} at the wavelength of 550 nm (bottom).

denser vegetation. Compared with an the Arctic station in Barrow (Alaska), the mean value of σ_{sca} at 550 nm estimated by us was 30% lower, and the value of σ_{abs} was about two times higher. The greater scattering coefficient at Barrow is probably due to stronger influence of sea salt particles and Arctic haze at Barrow (Delene and Ogren 2002). The higher absorption coefficients at Pallas as compared with those at Barrow are probably related to wintertime emissions of black carbon from continental areas (*see* below).

Of the tree stations in Finland, the backscattering fraction, b, at 550 nm, was the lowest at Pallas (0.13), about similar in Hyytiälä (0.14, Virkkula *et al*. 2011) and the highest in Kuopio (0.18, Leskinen *et al*. 2012). These differences further increased at the wavelength of 700 nm. The scattering Ångström exponent, $å_{sca}$, was also the highest (1.95) in Kuopio, and 1.7 at both Pallas and Hyytiälä. This is likely related to the fact that the measurements in Kuopio have a cut-off particle diameter of 2.5 μm: cutting off larger particles is expected to increase the values of b and $å_{sca}$. At the Arctic station in Barrow, the mean value of $å_{sca}$ was 1.1 (Delene and Ogren 2002) and thus clearly lower than that at Pallas. Delene and Ogren (2002) calculated $å_{sca}$ using the wavelengths 550 and 700 nm. In our analysis, the wavelengths selection did not affect the $å_{sca}$ result when testing two wavelength pairs (550 and 700 nm; 450 and 700 nm). The lower values $å_{sca}$ at Barrow as compared with those at Pallas indicate a more pronounced importance of larger particles in scattering at that site.

The absorption Ångström exponent, $å_{abs}$, can be used to characterize some of the aerosol absorbing species (Kirchstetter *et al*. 2004, Bergstrom *et al*. 2007). Black carbon (BC) aerosol has $å_{abs} = 1$. However, the wavelength dependence of absorption can be different to that of BC. For example, the vehicle exhaust typically has $å_{abs} \approx 1$ and biomass smoke can reach values in excess of 2. Mixed aerosols of BC and biomass smoke have values somewhere in the range 1–2. At Pallas, the average value of $å_{abs}$ was 1.1, which is about 20% lower than at Hyytiälä (Virkkula *et al*. 2011). This could be explained by the types of emissions and ageing processes of aerosols.

Aerosol optical properties in marine and continental air masses

Based on the history of measured air masses, about 45% of the air masses were defined as marine and about 34% as continental during the entire measurement period (Tables 2 and 3). As compared with the marine air, in the continental air masses σ_{sca} and σ_{abs} were higher by the factors of three and almost five, respectively. It is also interesting that in the marine air masses, $\mathring{a}_{sca}$ was clearly lower than in the continental air masses, which implies that the marine air masses were dominated by larger particles, possibly sea salt. The absorption Ångström exponent, $\mathring{a}_{abs}$, and the backscattering fraction, b, were about the same in the two air mass types. The single scattering albedo (SSA) was slightly lower in the continental air as compared with that in the marine air, and this difference was somewhat greater when calculated from monthly-averaged data. This is suggestive of low SSA values during winter because the monthly averaging corrects data gaps which were more frequent in winter.

In the continental air masses, the mean value of σ_{sca} was quite similar to that measured in Kuopio (about 10% higher, Leskinen *et al*. 2012), but clearly lower than that at the more southern Hyytiälä station (about 30% lower, Virkkula *et al*. 2011). The absorption coefficients in the continental air masses were about half of those measured in Hyytiälä. The average value of $\mathring{a}_{sca}$ of 2.0 in the continental air was close to the value of 1.95 measured in Kuopio, while in Hyytiälä it was only 1.7. Keeping in mind the fact that in Kuopio the aerosol inlet has a cut-off diameter of 2.5 μm, it is clear that smaller particles dominate scattering in the continental air.

Seasonal cycles

Seasonal cycles were analyzed from the hourly-averaged data classified according to the measurement month. Both scattering and absorption coefficients showed a clear seasonal cycle (Fig. 4), the monthly-minimum to monthly-maximum range being 3.0–10.5 Mm^{-1} for σ_{sca} and 0.38–1.46 Mm^{-1} for σ_{abs}. The phases of the annual cycle of these two quantities were, however, different. The minimum values of σ_{sca} and σ_{abs} were observed at about the same time in late autumn (November), whereas the maximum of σ_{sca} took place in late summer (August) and that of σ_{abs} in winter (February). The low values of both quantities in autumn and early winter were related to frequent precipitation events that were washing the atmosphere from aerosols. The high values of σ_{sca} in summer were probably related to biogenic organic aerosol from natural sources.

The seasonal cycle of σ_{abs} at Pallas was similar to that in Kuopio and Hyytiälä, with all these stations having a maximum in absorption during cold, winter months. The seasonal cycle of σ_{sca} at Pallas was, however, somewhat different from that at other stations in Finland. In Kuopio and Hyytiälä, σ_{sca} peaked in February and March, respectively, and had the lowest values in summer when at Pallas σ_{sca} reached its maximum. The seasonal variation of σ_{sca} at Pallas differed also clearly from that at the Arctic Barrow station in Alaska, where the maximum scattering values were measured in January and February and minimum in June. The seasonal variation of σ_{abs} was similar at Barrow and Pallas.

The seasonal cycle of the backscattering fraction, b, at Pallas was quite modest (Fig. 4). The minimum values of about 0.11 were found in winter months (January and February) and the maximum values of about 0.13 were observed in summer (July). The higher summer values were probably caused by the smaller mean particle sizes during the summer months as compared with those in winter. In summer, small secondary aerosol particles, probably biogenic organic aerosol from natural sources, were dominating the particle number size distribution and scattering (Tunved *et al*. 2006, Lihavainen *et al*. 2009).

The single scattering albedo, SSA, had a very clear seasonal cycle (Fig. 4). During the winter when scattering was low and absorption high, the SSA reached its lowest monthly-mean values of about 0.88. The highest values of about 0.95 were observed during summer when scattering had clearly the highest values and absorption was at the minimum.

The frequencies of the continental and marine air masses during the periods of the nephelometer (Fig. 5a) or aethalometer (Fig. 5d) measurements were quite similar: the marine air masses were

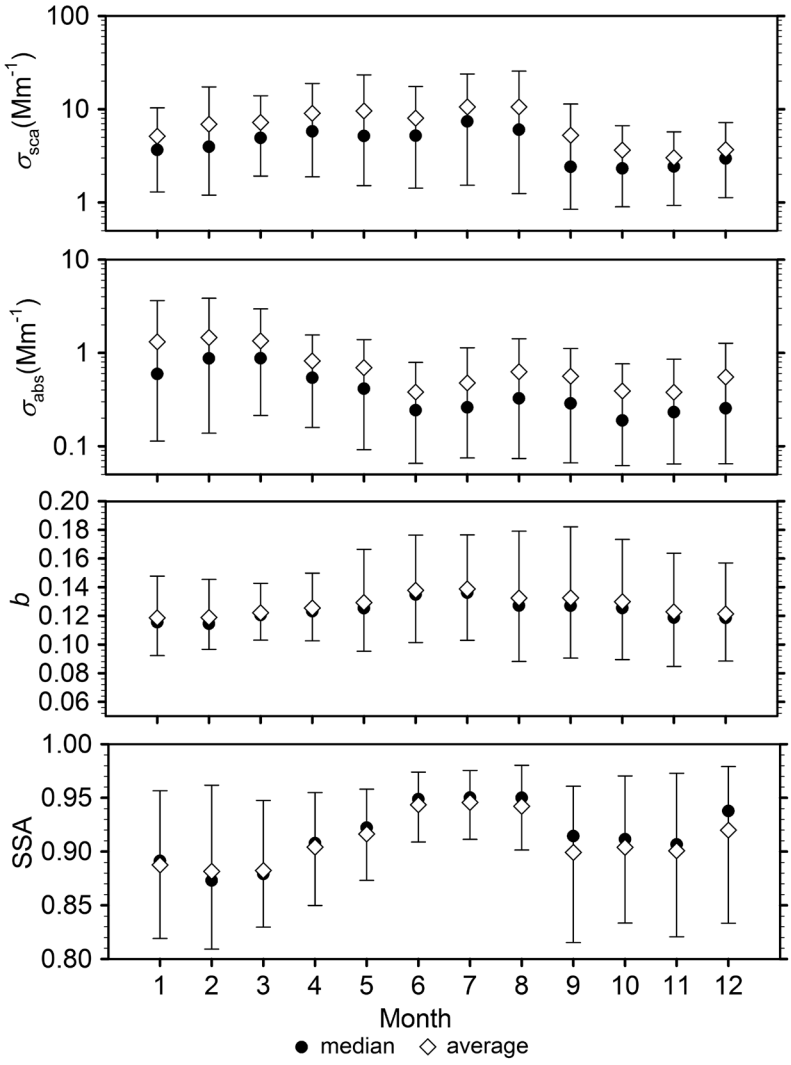

Fig. 4. Seasonal cycles of scattering coefficient, σ_{sca}, absorption coefficient σ_{abs}, backscattering fraction, *b,* and single scattering albedo (SSA) at the wavelength of 550 nm. Diamonds represent the averages, circles represent medians and bars represent the 10–90 percentile range.

prevailing during autumn and winter, whereas during summer these frequencies were quite even. The seasonal cycles of aerosol optical properties of the two air mass types differed clearly. The seasonal cycle of σ_{sca} in the continental air masses resembled that in the whole data set, except that the values were greater. In the marine air masses, the maximum value of σ_{sca} was observed in April, which could be a sign of the Arctic haze phenomenon (e.g. Law and Stohl 2007, Quinn *et al*. 2002). Particle sources in the continental air differ from those in the marine air and, especially during summer, biogenic organic aerosol from natural sources dominated the continental aerosol at Pallas (Lihavainen *et al*. 2009, Tunved *et al*. 2006). The impact of biogenic organic aerosol could also be distinguished in the marine air masses during summer, and a more detailed analysis of the effect of natural sources on the scattering coefficient in the marine air masses can be found in Lihavainen *et al*. (2009). The amplitude of the seasonal cycle was very strong in the continental air masses, as the values of σ_{sca} in late summer (16.9 Mm^{-1}) were more that four times higher than those in late autumn (3.6 Mm^{-1}).

Similar to σ_{sca}, the seasonal cycles of the absorption coefficient were clearly different in the two air mass types. In the marine air, the maximum value of σ_{abs} was observed in March, coincident with the maximum value of σ_{sca} in

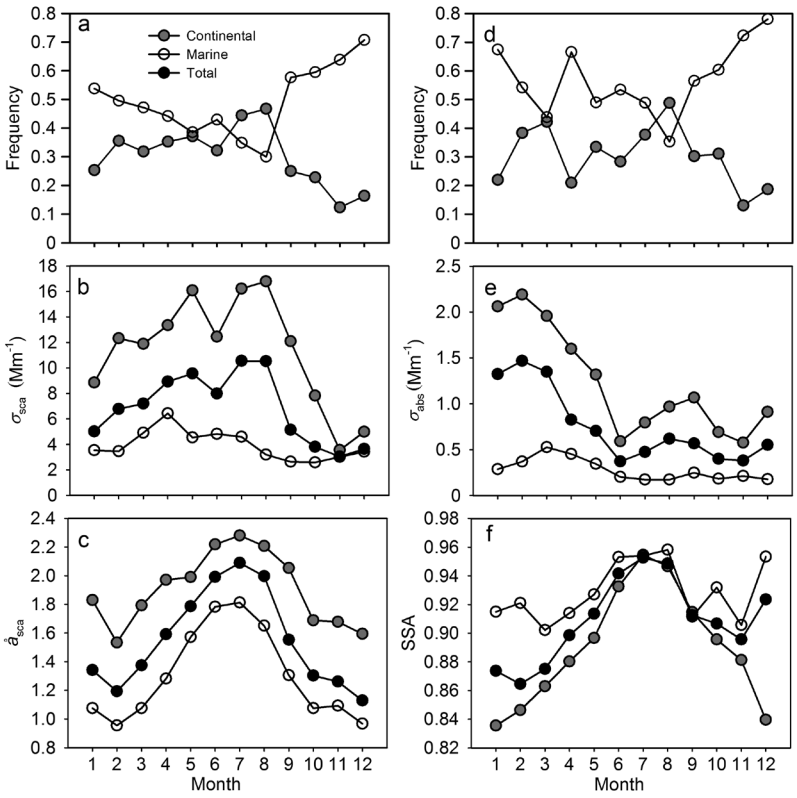

Fig. 5. Seasonal cycles as monthly averages: (**a**) the frequency of continental and marine air masses during the measurement period 2001–2010, (**b**) scattering coefficient, (**c**) σ_{sca}, scattering Ångström exponent, $\mathring{a}_{sca}$, (**d**) frequency of continental and marine air masses from 2005 to 2010, (**e**) absorption coefficient, σ_{abs}, and (**f**) single scattering albedo, SSA. All values are given at the wavelength of 550 nm.

spring, possibly due to the Arctic haze. In the continental air, the seasonal cycle of σ_{abs} was very pronounced, with high values from December to May and a maximum in January, yet this cycle was very different from that of σ_{sca}. This behavior could be explained with anthropogenic aerosol sources, most probably from residential combustion that produces absorbing aerosols during cold, winter months in Finland (Karvosenoja *et al*. 2011). However, it is still unknown whether during winter absorbing aerosols originate mostly from Finland or other parts of Europe. Hyvärinen *et al*. (2011) made a source region analysis with black carbon data from five measurement stations in Finland. Their analysis, though qualitative, showed that major sources of black carbon measured in Finland during the winter months were in areas around St. Petersburg and eastern Europe. The monthly-average values of σ_{abs} in the continental air masses varied from 0.6 Mm^{-1} (June) to 2.2 Mm^{-1} (February).

The scattering Ångström exponent, $\mathring{a}_{sca}$, had low values during summer in both air masses types as well as in the whole data set (Fig. 5c). The variation in monthly-mean values of $\mathring{a}_{sca}$ was slightly larger in the marine air masses (0.96–1.81) than in the continental air masses (1.53–2.28). This inter-annual variation is indicative of changes in the relative contribution of different-size particles to scattering. During winter when $\mathring{a}_{sca}$ had low values, the size distribution was dominated by large aerosols, most probably from primary emissions. In contrast, during summer the smaller secondary biogenic organic aerosols dominated the scattering.

As expected from seasonal cycles of the scattering and absorption coefficient, the SSA had low values during cold months from November to May. Again, this implies aerosols from anthropogenic sources, such as residential wood combustion. The seasonal variation of The SSA was quite noticeable in continental air masses, with monthly-mean values ranging from 0.84 to 0.95 (Fig. 5f). Heating by combustion is not necessary in summer which, together with increased amounts of biogenic organic aerosol in the conti-

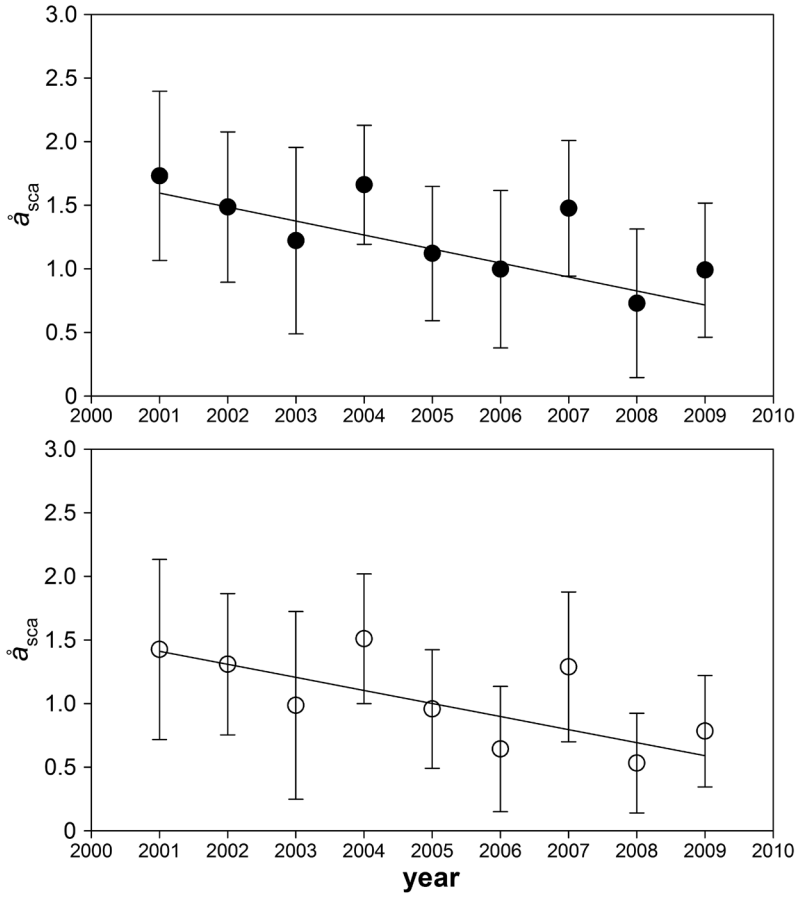

Fig. 6. Trends in wintertime (January–February) Ångström exponent, $å_{sca}$, from 2001 to 2010 in the whole data set (top), and marine air masses (bottom). Error bars are standard deviations, and the solid lines are linear fittings.

nental air masses (Lihavainen *et al*. 2009), leads to high values of the SSA in that time of the year. The seasonal cycle of the SSA in the marine air resembled that in the continental air, but its amplitude was smaller.

Long-term trends

A long-term trends in aerosol optical properties were extensively studied by Collaud Coen *et al*. (2013) at several stations around the world, including the Pallas GAW station. They carried out several analyses and did not find any significant long-term trend for the scattering coefficient at Pallas. However, they found a negative trend in the backscattering fraction and the scattering Ångström exponent. These trends were confirmed in our analysis. We extended the analysis to investigate how these trends were divided between the marine and continental cases in different seasons. Analyses were done only for scattering properties because the time series of the absorption coefficient was too short.

The scattering coefficient, σ_{sca}, did not have a significant trend in any air mass type or season, and the only quantity having a significant trend outside the winter or spring period was $å_{sca}$ (autumn, marine air masses). In winter, both b and $å_{sca}$ showed significant decreasing trends in the marine air masses and the whole data set (Table 4 and Fig. 6). The decrease in $å_{sca}$ in winter in the marine air and in the whole data set was quite substantial, being over 50% during the 10-year period. The corresponding decrease in b was modest, about 18% in the marine air masses and about 12% in the whole data set. In spring, only the backscattering fraction showed a decreasing trend and the decrease was clearly lower than that in winter. Collaud Coen *et al*.

(2013) found a decrease of about 9%–11% in $å_{sca}$ in their analysis for all the seasons, the exact value depending on the method used. They also found that at Barrow (Alaska) a similar decreasing trend in the backscattering fraction and much stronger decreasing trend in $å_{sca}$ was observed. The influence of a decreasing backscattering fraction on the direct radiative forcing by aerosols can be considered negligible due to the very low sun elevation and a very short duration of the day during winter.

Northern marine air masses dominated during winter (Fig. 5) and had a strong influence on the whole data set. The wintertime value of $å_{sca}$ correlated, though not very strongly (Pearson's r = –0.6), with the fraction of marine air masses. The fraction of marine air masses during winters increased slightly during the measurement period, though the correlation was quite moderate (Pearson's r = 0.5). Both $å_{sca}$ and b are size-dependent variables. A decrease in $å_{sca}$ indicates that the scattering coefficient becomes more sensitive to particles at the larger end of the accumulation mode (0.5 μm < particle diameter < 0.8 μm) (Collaud Coen *et al.* 2007). These larger particles also scatter relatively more light forward than smaller particle do (e.g. Seinfeld and Pandis 1998), so the backscattering fraction decreases when the particle number size distribution is shifted towards larger sizes. Some of the observed decrease in $å_{sca}$ and b might be explained by the slight increase in the fraction of marine air masses. The reason why these variables decreased with time in both marine and continental air masses might be the changing emission structure. The decrease in SO_2 emissions due to air quality legislation at lower latitudes and its effects to scattering coefficient were discussed by Collaud Coen *et al.* (2013), who also observed a decreasing trend of σ_{abs} at Barrow. It is possible that the effect of the decrease is so small at higher latitudes that it does not show up in σ_{sca}, but becomes noticeable only in the size-dependent variables. A decrease can also be seen in particulate sulphate concentrations at Pallas within the EMEP program (Ruoho-Airola *et al.* 2015). The decrease in SO_2 emissions might have an effect when more pollutants reach Arctic during the Arctic haze period. During late spring and summer, any signal of decreasing SO_2 emissions to scattering variables is probably small as compared with the biogenic organic aerosol production. It could also be hypothesized that the increases in amount and type of precipitation affected the observed decreases in b and $å$ (Ruoho-Airola *et al.* 2015).

Summary and conclusions

The mean absorption and scattering coefficients measured at the Pallas GAW station were lower than the corresponding values reported for other locations in Finland. As compared with the Arctic station Barrow in Alaska, scattering coefficients at Pallas were slightly lower while the absorption coefficients were slightly higher. The higher scattering coefficients at Barrow are probably caused by sea salt and Arctic haze which affect the aerosol population stronger at Barrow than at Pallas (Delene and Ogren 2002). The higher absorption coefficients at Pallas were probably related to wintertime emissions of black carbon from continental areas. Absorption coefficients should be, however, compared with caution because they were measured with different methods and different corrections were applied to the data.

Table 4. Sen's slope estimates for the backscatter fraction, b, and Ångström exponent of scattering, $å_{sca}$, as a function of time. Slope estimates were made for all the data and for the marine and continental cases separately. The units of the slopes are year^{-1} for b and $å_{sca}$. Only values for significant trends (at $p < 0.05$) are presented.

	All data		Marine		Continental	
	b	$å_{sca}$	b	$å_{sca}$	b	$å_{sca}$
Winter	–0.0022	–0.110	–0.0023	–0.103	–	–
Spring	–0.0014	–	–0.0013	–	–0.0015	–
Autumn	–	–	–	–0.078	–	–

There was a clear seasonal cycle in both scattering and absorption coefficient, but these cycles were different. The scattering coefficient had the highest values during summer and lowest during late autumn and early winter, whereas the absorption coefficient had the lowest values during summer and highest during winter. Our results suggest that the scattering coefficient measured at Pallas was affected mostly by natural emissions that tend to be highest in summer during the period of vegetation growth. The aerosols that affect absorption, in contrast, seemed to be mostly from anthropogenic sources, such as residential wood combustion that is common during cold, winter months. It is also noteworthy that the seasonal cycle of the scattering coefficient was different at Pallas than in other Finnish stations or at Barrow.

Aerosol particles were darker in winter, i.e. their single scattering albedo (SSA) was low, and brighter in summer (low SSA). The dark, winter aerosols do not have direct climate effects until the late winter or spring after the polar night. When deposited onto snow, these aerosols can induce an additional climate effect through surface albedo change and melting of snow.

The Arctic haze phenomenon was observed also at Pallas during March and April, the typical Arctic haze period. Near the ground surface, the haze tends to disappear in April, whereas at higher altitudes it may persist as layers until May (Law and Stohl 2007). In the marine (northern) air masses arriving at Pallas during March and April, the Arctic haze increased absorption by almost 80% and scattering by about 50% as compared with the corresponding annual-average values. The signal of the Arctic haze was not visible in the whole data set (undivided between different source areas), since these data were dominated by the relatively large scattering coefficients from continental sources. As Pallas is just above the Arctic Circle, it is hard to distinguish between the Arctic haze and regional or long-range-transported aerosol from combustion and energy production during winter.

We did not observe any statistically significant long-term trend in the scattering coefficient. This is consistent with the study by Collaud Coen *et al*. (2013) who instead found decreasing trends in the backscattering fraction and scattering Ångström exponent. We studied this behavior extensively and found that the decreasing trend took place in winter only and was stronger in the marine air masses. The decrease in the backscattering fraction had a negligible effect on the direct aerosol forcing due to the low sun elevation angle and very short duration of the day in winter. The decrease in the Ångström exponent was very substantial, about 50% over the 10-year measurement period. A fraction of the observed trends in the whole data could be connected with the slight increase in the frequency of air masses originating from marine areas. This was, however, not the sole explanation, so we hypothesize that the changing emission structure was the main cause for the observed trends.

Acknowledgements: This work was supported by the Academy of Finland as part of the Centre of Excellence program (project no. 1118615), FICCA program (project no. 140867) and Arctic Absorbing Aerosols and Albedo of Snow (project no. 3162), project Greenhouse gas, aerosol and albedo variations in the changing Arctic (project number 269095) as well as by the European Commission 6th framework program project EUCAARI (contract 036833-2) and EU LIFE+ project MACEB (project no. LIFE09 ENV/FI/000572).

References

Aaltonen V., Lihavainen H., Kerminen V.-M., Komppula M., Hatakka J., Eneroth K., Kulmala M. & Viisanen Y. 2006. Measurements of optical properties of atmospheric aerosols in Northern Finland. *Atmos. Chem. Phys*. 6: 1155–1164.

Anderson T.L. & Ogren J.A. 1998. Determining aerosol radiative properties using the TSI 3563 integrating nephelometer. *Aerosol Sci. Technol*. 29: 57–69.

Anderson T.L., Covert D.S., Marshall S.F., Laucks M.L., Charlson R.J., Waggoner A.P., Ogren J.A., Caldow R., Holm R.L., Quant F.R., Sem G.J., Wiedensohler A., Ahlquist N.A. & Bates T.S. 1996. Performance characteristics of a high-sensitivity, three-wavelength, total scatter/backscatter nephelometer. *J. Atmos. Oceanic Technol*. 13: 967–986.

Baron P.A. & Willeke K. 2001. *Aerosol measurement*, 2nd ed. John Wiley, Hoboken, NJ.

Beine H.J., Engardt M., Jaffe D.A., Hov Ø., Holmén K. & Stordal F. 1996. Measurements of NO_x and aerosol particles at the Ny-Ålesund Zeppelin mountain station on Svalbard: influence on regional and local pollution sources. *Atmos. Environ*. 30: 1067–1079.

Bellouin N., Jones A., Haywood J. & Christopher S.A. 2008. Updated estimate of aerosol direct radiative forcing from satellite observations and comparison against the Hadley Centre climate model. *J. Geophys. Res*. 113, D10205,

doi:10.1029/2007JD009385.

Bergstrom R.W., Pilewskie P., Russell P.B., Redemann J., Bond T.C., Quinn P.K. & Sierau B. 2007. Spectral absorption properties of atmospheric aerosols. *Atmos. Chem. Phys.* 7: 5937–5943.

Charlson R.J., Schwartz S.E., Hales J.M., Cess R.D., Coakley Jr. J.A., Hansen J.E. & Hoffman D.J. 1992. Climate forcing by anthropogenic aerosols. *Science* 255: 423–430.

Collaud Coen M., Weingartner E., Nyeki S., Cozic J., Henning S., Verheggen B., Gehrig R. & Baltensperger U. 2007. Long-term trend analysis of aerosol variables at the high-alpine site Jungfraujoch. *J. Geophys. Res.* 112, D13213, doi:10.1029/2006JD007995.

Collaud Coen M., Andrews E., Asmi A., Baltensperger U., Bukowiecki N., Day D., Fiebig M., Fjaeraa A.M., Flentje H., Hyvärinen A., Jefferson A., Jennings S.G., Kouvarakis G., Lihavainen H., Lund Myhre C., Malm W.C., Mihapopoulos N., Molenar J.V., O'Dowd C., Ogren J.A., Schichtel B.A., Sheridan P., Virkkula A., Weingartner E., Weller R. & Laj P. 2013. Aerosol decadal trends — Part 1: *In-situ* optical measurements at GAW and IMPROVE stations. *Atmos. Chem. Phys.* 13: 869–894.

Delene D.J. & Ogren J.A. 2002. Variability of aerosol optical properties at four North American surface monitoring sites. *J. Atmos. Sci.* 59: 1135–1150.

Hatakka J., Aalto T., Aaltonen V., Aurela M., Hakola H., Komppula M., Laurila T., Lihavainen H., Paatero J., Salminen K. & Viisanen Y. 2003. Overview of the atmospheric research activities and results at Pallas GAW station. *Boreal Env. Res.* 8: 365–384.

Gilbert R.O. 1987. Statistical methods for environmental pollution monitoring. Van Nostrand Reinhold, New York.

Hyvärinen A.-P., Kolmonen P., Kerminen V.-M., Virkkula A., Leskinen A., Komppula M., Hatakka J., Burkhart J., Stohl A., Aalto P., Kulmala M., Lehtinen K.E.J., Viisanen Y. & Lihavainen H. 2011. Aerosol black carbon at five background measurement sites over Finland, a gateway to the Arctic. *Atmos. Environ.* 45: 4042–4050.

IPCC 2013. *Climate change 2013: the physical science basis*. Contribution of Working Group I to the Fifth Assessment Report of the Intergovernmental Panel on Climate Change, Cambridge University Press, Cambridge, United Kingdom and New York.

Karvosenoja N., Kangas L., Kupiainen K., Kukkonen J., Karppinen A., Sofiev M., Tainio M., Paunu V.-V., Ahtoniemi P., Tuomisto J.T. & Porvari P. 2011. Integrated modeling assessments of the population exposure in Finland to primary $PM_{2.5}$ from traffic and domestic wood combustion on the resolutions of 1 and 10 km. *Air Qual. Atmos. Health* 4: 179–188.

Komppula M., Lihavainen H., Kerminen V.-M., Kulmala M. & Viisanen Y. 2005. Measurements of cloud droplet activation of aerosol particles at a clean subarctic background site. *J. Geophys. Res.* 110, D06204, doi:10.1029/2004JD005200.

Kirchstetter, T.W., Novakov T. & Hobbs P.V. 2004. Evidence that the spectral dependence of light absorption by aerosols is affected by organic carbon. *J. Geophys. Res.* 109, D21208, doi:10.1029/2004JD004999.

Law K.S. & Stohl A. 2007. Arctic Air Pollution: Origins and Impacts. *Science* 315: 1537–1540.

Leskinen A., Arola A., Komppula M., Portin H., Tiitta P., Miettinen P., Romakkaniemi S., Laaksonen A. & Lehtinen K.E.J. 2012. Seasonal cycle and source analyses of aerosol optical properties in a semi-urban environment at Puijo station in eastern Finland. *Atmos. Chem. Phys.* 12: 5647–5659.

Lihavainen H., Kerminen V.-M., Tunved P., Aaltonen V., Arola A., Hatakka J., Hyvärinen A. & Viisanen Y. 2009. Observational signature of the direct radiative effect by natural boreal forest aerosols and its relation to the corresponding first indirect effect. *J. Geophys. Res.* 114, D20206, doi:10.1029/2009JD012078.

Mielonen T., Aaltonen V., Lihavainen H., Hyvärinen A.-P., Arola A., Komppula M. & Kivi R. 2013. Biomass burning aerosols observed in northern Finland during the 2010 wildfires in Russia. *Atmosphere* 4: 17–34.

Müller T., Henzing J. S., de Leeuw G., Wiedensohler A., Alastuey A., Angelov H., Bizjak M., Collaud Coen M., Engström J.E., Gruening C., Hillamo R., Hoffer A., Imre K., Ivanow P., Jennings G., Sun J.Y., Kalivitis N., Karlsson H., Komppula M., Laj P., Li S.-M., Lunder C., Marinoni A., Martins dos Santos S., Moerman M., Nowak A., Ogren J. A., Petzold A., Pichon J.M., Rodriquez S., Sharma S., Sheridan P.J., Teinilä K., Tuch T., Viana M., Virkkula A., Weingartner E., Wilhelm R. & Wang Y. Q. 2011. Characterization and intercomparison of aerosol absorption photometers: result of two intercomparison workshops. *Atmos. Meas. Tech.* 4: 245–268.

Ruoho-Airola T., Anttila P., Hakola H., Ryyppö T. & Tuovinen J.-P. 2015. Trends in the bulk deposition and atmospheric concentration of air pollutants in the Finnish 1 Integrated Monitoring catchment Pallas during 1992–2012. *Boreal Env. Res.* 20: 553–569.

Quinn P.K., Miller T.L., Bates T.S., Ogren J.A., Andrews E. & Shaw G.E. 2002. A three-year record of simultaneously measured aerosol chemical and optical properties at Barrow, Alaska. *J. Geophys. Res.* 107, doi:10.1029/2001JD001248.

Quinn P.K., Shaw G., Andrews E., Dutton E.G., Ruoho-Airola T. & Gong S.L. 2007. Arctic haze: current trends and knowledge gaps. *Tellus* 59B: 99–114.

Rizzo L.V., Artaxo P. , Müller T., Wiedensohler A., Paixão M. , Cirino G.G., Arana A., Swietlicki E., Roldin P., Fors E.O., Wiedemann K.T., Leal L.S.M. & Kulmala M. 2013. Long term measurements of aerosol optical properties at a primary forest site in Amazonia. *Atmos. Chem. Phys.* 13: 2391–2413.

Seinfeld J.H. & Pandis S.N. 1998. *Atmospheric chemistry and physics: From air pollution to climate change*. John Wiley & Sons, New York.

Sheridan P.J. & Ogren J.A. 1999. Observations of the vertical and regional variability of aerosol optical properties over central and eastern North America. *J. Geophys. Res.* 104: 16793–16805.

Shindell D. & Faluvegi G. 2009. Climate response to regional radiative forcing during the twentieth century. *Nature Geosci.* 2: 294–300.

Stohl A. & Seibert P. 1998. Accuracy of trajectories as deter-

mined from the conservation of meteorological tracers. *Q. J. R. Meteorol. Soc.* 124: 1465–1484.

Treffeisen R., Herber A., Ström J., Shiobara M., Yamanouchi T., Yamagata S., Holmén K., Kriews M. & Schrems O. 2004. Interpretation of Arctic aerosol properties using cluster analysis applied to observations in the Svalbard area. *Tellus* 56B: 457–476.

Tunved P., Hansson H.-C., Kerminen V.-M., Ström J., Dal Maso M., Lihavainen H., Viisanen Y., Aalto P.P., Komppula M. & Kulmala M. 2006. High natural aerosol loading over boreal forests. *Science* 14: 261–263.

Vaishya A., Jennings S.G. & O'Dowd C.D. 2012. Wind-driven influences on aerosol light scattering in north-east Atlantic air. *Geophys. Res. Lett.* 39, L05805, doi:10.1029/ 2011GL050556.

Weingartner E., Saathoff H., Schnaiter M., Streit N., Bitnar B. & Baltensperger U. 2003. Absorption of light by soot particles: determination of the absorption coefficient by means of aethalometers. *J. Aerosol Sci.* 34: 1445–1463.

Virkkula A., Backman J., Aalto P.P., Hulkkonen M., Riuttanen L., Nieminen T., Dal Maso M., Sogacheva L., de Leeuw G. & Kulmala M. 2011. Seasonal cycle, size dependencies, and source analyses of aerosol optical properties at the SMEAR II measurement station in Hyytiälä, Finland. *Atmos. Chem. Phys.* 11: 4445–4468.

Witte J.C., Douglass A.R., da Silva A., Torres O., Levy R. & Duncan B.N. 2011. NASA A-Train and Terra observations of the 2010 Russian wildfires. *Atmos. Chem. Phys.* 11: 9287–9301.

Zhou C., Penner J.E., Ming Y. & Huang X.L. 2012. Aerosol forcing based on CAM5 and AM3 meteorological fields. *Atmos. Chem. Phys.* 12: 9629–9652.